Direct electrochemistry of nanoparticulate Fe$_2$O$_3$ in aqueous solution and adsorbed onto tin-doped indium oxide*

Katy J. McKenzie and Frank Marken[‡]

Department of Chemistry, Loughborough University, Loughborough, Leicestershire, LE11 3TU, UK

Abstract: Nanoparticulate iron oxides occur naturally, for example, in soil, water, and in the cytoplasm of living cells. The redox properties and detection of these nanoparticles are therefore of considerable importance. Understanding and mimicking nanoparticle-based redox reactions may lead to new types of water-based electrochemical processes. In this study, the electrochemical detection of 4–5 nm diameter Fe$_2$O$_3$ nanoparticles dissolved in aqueous buffer solutions is investigated as a model system.

Voltammetric experiments with nanoparticulate Fe$_2$O$_3$ are reported based on two complementary approaches: (i) Fe$_2$O$_3$ nanoparticles adsorbed onto tin-doped indium oxide (ITO) electrodes are shown to give well-defined voltammetric reduction responses and (ii) hydrodynamic voltammety in the presence of fast (24 kHz ultrasound-enhanced) mass transport is shown to allow the direct detection of Fe$_2$O$_3$ nanoparticles in solution. Both the adhesion and the electrochemical reactivity of Fe$_2$O$_3$ nanoparticles at ITO electrode surfaces are strongly affected by the solution composition and the pH.

INTRODUCTION

Iron oxide nanoparticles are an important component in natural and industrial processes occurring, for example, in the form of ferrihydrite iron storage (ferritin) particles [1], as colloids in oceans and groundwater [2], and in the form of sludge in water and mineral processing. Important naturally occurring processes involving Fe$_2$O$_3$ nanoparticles are the surface adsorption of trace metals and organic matter [3], photoexcitation and the photochemically induced transfer of electrons [4,5], and direct electron transfer [6].

Although the rate of mass transport (diffusion) for nanoparticulate redox systems is comparatively slow, one particular benefit of nanoparticle-based electrochemical processes is the possibility to work with aqueous solutions of materials, which are in water inherently insoluble. In this way, materials soluble only in organic solvents may be processed in solid colloidal form in aqueous solutions. Considerable interest exists in nanoparticles adsorbed onto electrode surfaces [7,8] but relatively little is known to date about electrochemical processes involving dissolved nanoparticulate systems [9–11]. A brief historical account and outline of the problem of the particle-to-electrode interaction has been given recently [12]. Here, Fe$_2$O$_3$ nanoparticles are employed as a model system, and electrochemical responses are compared for particles in adsorbed and in dissolved state.

The various known types of iron oxides [13] are of considerable technological importance, and several studies have addressed their solid-state electrochemical properties [14]. The interaction of Fe_2O_3 with mercury electrode surfaces [15] and mechanistic aspects of the reductive dissolution of Fe_2O_3 from a carbon paste electrode have been reported [16,17]. Recently, Grygar and coworkers [18–20] published a detailed comparison of mechanistic features for the reductive dissolution of a range of different iron oxides.

In this study, preliminary results are reported for two novel approaches employed to investigate the electrochemical properties of nanoparticulate iron oxide: (i) the direct voltammetry of Fe_2O_3 nanoparticles adsorbed onto tin-doped indium oxide (ITO) electrodes is reported and (ii) the ultrasound enhanced voltammetry of colloidal Fe_2O_3 in aqueous solution is shown to result in well-defined quasi-steady-state responses.

EXPERIMENTAL

Chemical reagents

$FeCl_3.6H_2O$ (Fisher), ethylenediaminetetraacetic acid (EDTA) (Aldrich), KH_2PO_4, K_2HPO_4, KOH (Fisons), $HClO_4$ (60%, Aldrich), KCl, $Ru(NH_3)_6Cl_3$ (BDH) were obtained commercially and used without further purification. Filtered and demineralized water was taken from an Elgastat water purification system (Elga, High Wycombe, Bucks, UK) with at least 18 MOhm cm resistivity.

Colloidal iron oxide was prepared following a literature procedure established by Mulvaney *et al.* [21] and Sorum [22]. During this synthesis, hydrous ferric oxide (HFO) is probably formed initially, but slow recrystallization occurs. The product was identified as predominantly α-Fe_2O_3 [21]. Briefly, the procedure consists of dropwise addition of an aqueous solution of $FeCl_3$ into boiling water to give a colloidal solution 2 mM in Fe. After dialysis against aqueous $HClO_4$ (pH 3.5), the solution was stable and was stored in a polyethylene bottle. A TEM image (see Fig. 1) shows uniformly sized Fe_2O_3 nanoparticles with an average diameter of 4 to 5 nm.
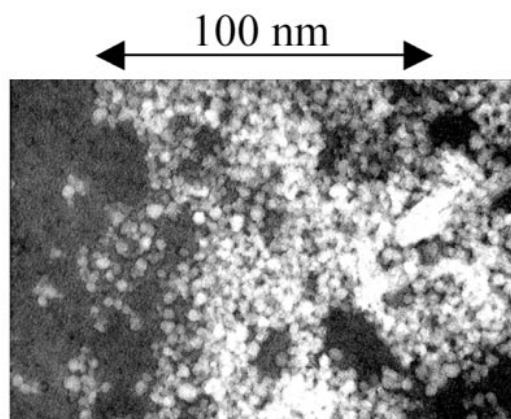

Fig. 1 TEM image of Fe_2O_3 nanoparticles with an average diameter of 4–5 nm.

Instrumentation

Electrochemical measurements were performed with a PC-controlled Autolab potentiostat system (Ecochemie, Netherlands). Experiments were conducted in a conventional three-electrode configuration

with a saturated Calomel reference electrode (SCE, Radiometer, Copenhagen) and a Pt gauze counter electrode. As the working electrode, an ITO-coated glass electrode (Image Optics Components Ltd., Basildon, Essex) was employed. Test experiments with other types of electrodes (glassy carbon, Pt, Au) showed that the nanoparticle–electrode interaction is very sensitive to the type of electrode material employed and ITO was found to be superior. ITO electrodes were cut into 4-mm-wide plates and covered with "Magic Tape" (3M) to leave a 3×4 mm electrode area exposed to the aqueous solution. The electrode surface was cleaned by ultrasound treatments in ethanol (5 min) and in aqueous 10 mM EDTA (5 min) followed by rinsing with copious amounts of water. All experiments were conducted in thoroughly argon-de-aerated solutions (Pureshield, BOC) at a temperature of 22 ± 2 °C.

For ultrasound-enhanced voltammetry experiments, a Hielscher UPG 200 glass horn system with 13-mm-diameter horn emitter (24 kHz, 8 W cm^{-2}) was employed. The experimental conditions were similar to those described previously [23,24]. TEM images were obtained on a Jeol JEM100CX system operating at 100 kV.

RESULTS AND DISCUSSION

Voltammetry of Fe₂O₃ nanoparticles adsorbed onto ITO electrodes

Colloidal Fe₂O₃ in form of 4–5 nm-diameter-sized nanoparticles (see Fig. 1) is positively charged due to the point of zero charge (pzc) at approximately pH 8 [25]. The interaction of positively charged nanoparticles with the ITO electrode leads to rapid Fe₂O₃ adsorption at the interface. Figure 2A shows cyclic voltammograms obtained for the reduction of Fe₂O₃ nanoparticles adsorbed onto an ITO electrode (the ITO electrode was immersed for 1 min in the Fe₂O₃ sol and rinsed with water) and then
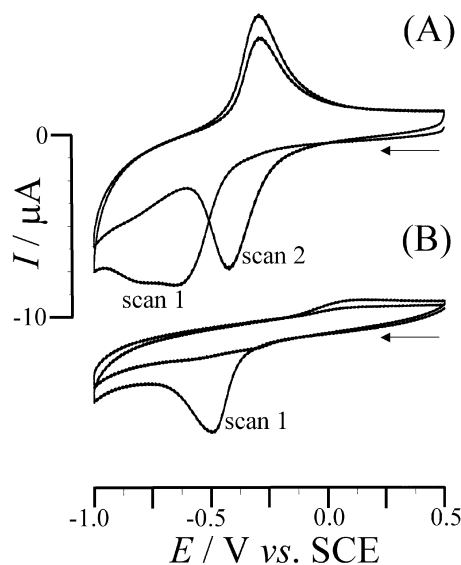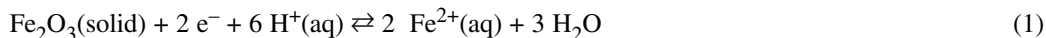

Fig. 2 Cyclic voltammograms (two cycles, scan rate 0.1 V s^{-1}) obtained for the reduction of Fe₂O₃ nanoparticles adsorbed (by immersion into a Fe₂O₃ sol 2 mM in Fe) onto a 3×4 mm^2 ITO electrode and immersed (A) in aqueous 0.1 M phosphate buffer at pH 8 and (B) in aqueous 0.1 M phosphate buffer at pH 8 containing 10 mM EDTA.

immersed in aqueous 0.1 M phosphate buffer solution at pH 8. The first cycle allows the direct reduction of Fe_2O_3 to be detected as a broad peak with E_p^{red} = –0.66 V vs. SCE (eq. 1).

$$Fe_2O_3(solid) + 2 e^- + 6 H^+(aq) \rightleftarrows 2 \ Fe^{2+}(aq) + 3 H_2O \tag{1}$$

In repeat experiments, the reduction peak is detected reproducibly. The charge under the peak determined by integration of the reduction peak in scan 1 (see Fig. 2A), 31 μC, can be used for the approximate calculation of the number of nanoparticles absorbed. Nanoparticles with a 4–5 nm diameter can be estimated (based on the density of haematite 5.24 g cm^{-3}) to contain approximately 2500 Fe atoms. The charge under the reduction peak is then consistent with 10^{11} nanoparticles or an area of approximately 10 nm × 10 nm per nanoparticle on the electrode surface. Therefore, approximately a monolayer packing of Fe_2O_3 nanoparticles on the surface of the ITO electrode is present.

After reversal of the scan direction (see Fig. 2A), an oxidation response is detected at E_p^{ox} = –0.30 V vs. SCE. Upon stirring the solution simultaneously to potential cycling, this oxidation process is absent. Therefore, it is attributed to a solution phase species, $Fe^{2+}(aq)$, being oxidized to solid $FePO_4$ [26] (eq. 2).

$$Fe^{2+}(aq) + HPO_4^{2-}(aq) \rightleftarrows FePO_4(solid) + e^- + H^+(aq) \tag{2}$$

The second cycle of the cyclic voltammetric experiment (see Fig. 2A) reveals the presence of solid $FePO_4$ at the surface of the ITO electrode, which is detected as a stripping response at E_p^{red} = –0.43 V vs. SCE. Figure 3 demonstrates that the voltammetric response detected for the reduction of Fe_2O_3 nanoparticles adsorbed onto an ITO electrode is strongly pH-dependent. Well-defined peak-shaped signals for the reduction of Fe_2O_3 freshly coated onto ITO electrodes are observed from pH 5 to 7. In more alkaline solutions, the reduction signal broadens and finally splits. The reduction peak is undergoing a shift of ca. 110 mV per pH unit, indicating a strong pH effect. The appropriate Nernst expression based on eq. 1 predicts a shift of 177 mV per pH unit (at 25 °C, compare Pourbaix diagram [27]), but it is likely that under the experimental conditions employed here, instead of $Fe^{2+}(aq)$, a phosphate complex of the type $Fe(OH)^+(aq)$ is formed consistent with a shift in equilibrium potential of only 118 mV per pH unit. Furthermore, the Pourbaix diagram for the Fe oxide system [27] is predicting more complex
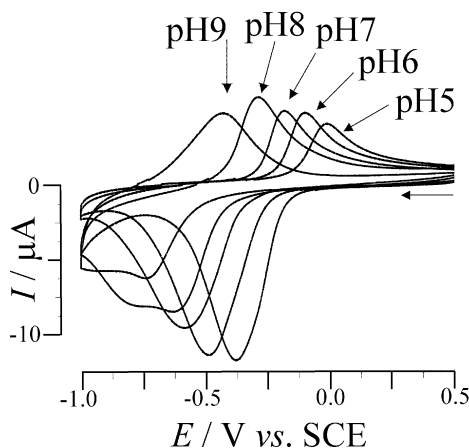

Fig. 3 Cyclic voltammograms (scan rate 0.1 V s^{-1}) obtained for the reduction of Fe_2O_3 nanoparticles adsorbed (by immersion into a Fe_2O_3 sol 2 mM in Fe) onto a 3 × 4 mm^2 ITO electrode and immersed in aqueous 0.1 M phosphate buffer at a range of different pH values. Only the first potential cycle obtained with freshly coated electrodes is shown.

processes involving an Fe$_3$O$_4$ intermediate at more alkaline pH. This could explain the more complex voltammetric response at pH > 7.

The redox system detected in the second and the following potential cycles is different compared to the process detected during the first reduction (see Fig. 2A). This voltammetric response corresponds to the chemically reversible reduction (E_p^{red} = –0.42 V vs. SCE at pH 8) and oxidation process (E_p^{ox} = –0.19 V vs. SCE at pH 8) given by eq. 2. A shift of the mid-potential, $\frac{1}{2}$ (E_p^{ox} + E_p^{red}), of approximately 60 mV per pH unit consistent with eq. 2 was detected over a pH range from pH 5 to 9. A scheme indicating the two types of redox processes encountered is shown in Fig. 4. The first reduction process (A) occurring at more negative potential is consistent with the reduction of Fe$_2$O$_3$. The second process (B) is chemically reversible and associated with the formation of solid FePO$_4$ at the electrode surface. The more negative potential for the reduction of Fe$_2$O$_3$ compared to FePO$_4$ is consistent with Fe$_2$O$_3$ being less soluble.
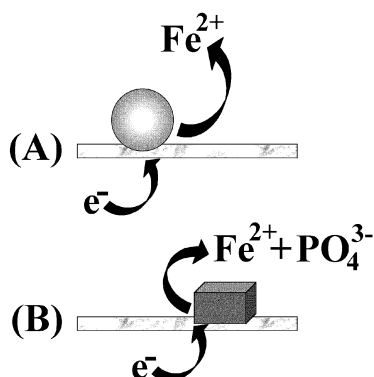

Fig. 4 Schematic representation of the reductive dissolution of Fe$_2$O$_3$ nanoparticles (A) and the reversible FePO$_4$ reduction process (B).

It is interesting to explore the effect of a multidentate trapping agent, such as ethylenediaminetetraacetic acid (EDTA), on the electrochemical response. Fe^{2+}(aq) generated from Fe$_2$O$_3$ during the reduction process, is captured by EDTA present in 10 mM concentration in the aqueous buffer solution. Figure 2B shows that the follow-up redox process given by eq. 2 is absent in the cyclic voltammogram obtained in the presence of EDTA. Under these conditions, the reduction of Fe$_2$O$_3$ nanoparticles adsorbed onto ITO is detected at E_p^{red} = –0.5 V vs. SCE. As expected, a slight shift to more positive potential occurs in the presence of the potent complexation reagent.

Solution-phase voltammetry of Fe$_2$O$_3$ nanoparticles
The accumulation of Fe$_2$O$_3$ nanoparticles by adsorption onto the electrode surface allows many aspects of redox reactivity to be explored. However, only nanogram quantities of Fe$_2$O$_3$ react, and only transient voltammetry-based experiments can be performed. An interesting complementary experimental approach is to investigate nanoparticles dissolved in the solution phase. One obstacle to this type of experiment is the low rate of diffusion of nanoparticles compared to the rate of diffusion for conventional molecules. For the Fe$_2$O$_3$ nanoparticles of 4 to 5 nm diameter studied here, the rate of diffusion may be estimated based on the Stokes–Einstein expression [28] (e. 3).

$$D = \frac{k\ T}{6\pi\eta\ r} \tag{3}$$

In this expression, the diffusion coefficient D for the nanoparticle can be calculated based on the temperature T, the viscosity $\eta = 10^{-3}$ Pa s (at 20 °C [29]), and the radius r for the particle. The result $D = 8.5 \, (\pm 1) \times 10^{-11}$ m^2 s^{-1} suggests that particles will diffuse considerably slower compared to conventional molecular redox systems.

Due to the slow rate of diffusion of nanoparticles in aqueous solutions and the high number of redox centres per nanoparticle, the direct solution-phase voltammetry of nanoparticles is dominated by adsorption effects. Signals very similar to those described above are detected. In order to detect nanoparticles without accumulation due to adsorption, an experimental approach has to be chosen with (i) a sufficiently high concentration of nanoparticles, (ii) small electrodes to improve the signal-to-background ratio, or (iii) very fast mass transport.

Here we are employing power ultrasound to drastically improve the rate of mass transport of nanoparticles toward the electrode surface. Figure 5 shows a schematic drawing of the experimental set-up with a 24 kHz glass horn system immersed into the sample solution and placed opposite the ITO working electrode at the bottom of the electrochemical cell. In this arrangement, the electrode is directly exposed to high intensity (5 mm electrode-to-horn distance, 8 W cm^{-2}) ultrasound resulting in agitation and cavitational cleaning [30]. A test redox system, the one-electron reduction of Ru(NH$_3$)$_6^{3+}$ in aqueous 0.1 M KCl (eq. 4), was employed to calibrate the rate of mass transport achieved under these conditions [31].

$$\text{Ru(NH}_3)_6{}^{3+}\text{(aq)} + e^- \rightleftarrows \text{Ru(NH}_3)_6{}^{2+}\text{(aq)} \tag{4}$$

Based on the Nernst diffusion layer expression for the mass transport limited current (eq. 5), I_{SONO}, and the diffusion coefficient for the Ru(NH$_3$)$_6^{3+}$ cation, $D = 0.91 \times 10^{-9}$ m^2 s^{-1} [32], an average diffusion layer thickness of $\delta = 3.5$ μm was determined independent of the concentration of the Ru(NH$_3$)$_6^{3+}$ complex.

$$I_{SONO} = \frac{n\,F\,D\,A\,c}{\delta} \tag{5}$$

In eq. 5, n is the number of electrons transferred per molecule diffusing to the electrode surface, F denotes Faraday's constant, A is the electrode area, and c is the bulk solution concentration. An aver-
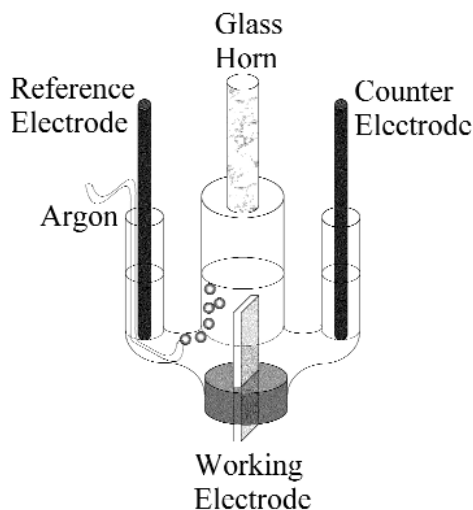

Fig. 5 Schematic drawing of the experimental set-up used for sonovoltammetric experiments with a glass immersion horn system placed opposite an ITO electrode in aqueous Fe$_2$O$_3$ nanoparticle containing solutions.

age diffusion layer thickness of $\delta = 3.5$ μm is consistent with fast mass transport and should allow well-defined voltammetric signals for the nanoparticle solution to be observed.

Figures 6A and 6B show cyclic voltammograms for the reduction of Fe$_2$O$_3$ nanoparticles (0.25 mM in Fe) in aqueous 0.1 M phosphate buffer (pH 7). In Fig. 6A, a voltammogram obtained under silent conditions is shown. The two pronounced reduction peaks can be attributed to the reduction of a FePO$_4$ deposit at the ITO electrode surface ($E_p^{red} = -0.32$ V vs. SCE) and the reduction of Fe$_2$O$_3$ nanoparticles adsorbed onto the ITO surface ($E_p^{red} = -0.62$ V vs. SCE). In the presence of 8 W cm^{-2} ultrasound (see Fig. 6B) both peaks show a dramatically reduced peak current due to ultrasound (i) removing adsorbed Fe$_2$O$_3$ nanoparticles, and (ii) effectively removing the soluble Fe^{2+}(aq) reduction product and preventing redeposition of FePO$_4$. However, experiments conducted over a range of different concentrations of Fe$_2$O$_3$ nanoparticles in aqueous phosphate buffer indicated that partial electrode passivation occurred, and reproducibility of results posed a problem even in the presence of ultrasound. The
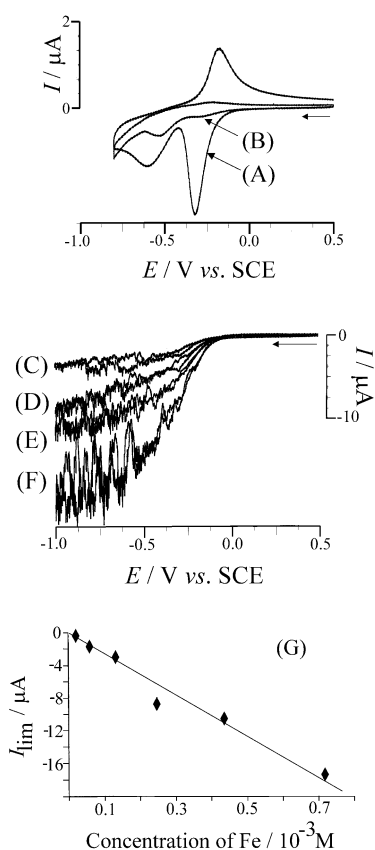

Fig. 6 Cyclic voltammograms obtained for the reduction of Fe$_2$O$_3$ (0.25 mM Fe) at a 3 × 4 mm^2 ITO electrode immersed in 0.1 M phosphate buffer solution (pH 7) in the absence (A) and in the presence (B) of power ultrasound (8 W cm^{-2}, 24 kHz, 5 mm electrode-to-horn distance). Cyclic sonovoltammograms (24 kHz, 5 mm horn-to-electrode distance, 8 W cm^{-2}, scan rate 0.1 V s^{-1}, background substracted) obtained for the reduction of Fe$_2$O$_3$ nanoparticles at a 3 × 4 mm^2 ITO electrode immersed in aqueous 0.1 M phosphate buffer at pH 5 containing 10 mM EDTA and a concentration of (C) 0.13 mM, (D) 0.25 mM, (E) 0.44 mM, and (F) 0.72 mM Fe in the form of Fe$_2$O$_3$ nanoparticles. The plot (G) shows data for the sonovoltammetric limiting current as a function of the Fe concentration in form of Fe$_2$O$_3$ nanoparticles.

passivation effect may in part be due to the very efficient accumulation of $FePO_4$ in the presence of fast mass transport. Therefore, experiments were conducted in the presence of 10 mM EDTA in the aqueous solution phase.

In a solution of Fe_2O_3 nanoparticles in 0.1 M phosphate buffer (pH 5) containing 10 mM EDTA, well-defined sonovoltammetric limiting currents are detected (see Fig. 6C to F). The foot of the voltammetric wave occurs at ca. –0.1 V vs. SCE consistent with the signal detected for the reduction of Fe_2O_3 at pH 5 as shown in Fig. 3. Therefore, the process detected is that described by eq. 1 followed by EDTA complexation of the product, $Fe^{2+}(aq)$. The limiting current increases approximately linearly with nanoparticle concentration from 0.03 to 0.72 mM Fe (see Fig. 6G). Data analysis of the sonovoltammetric limiting currents based on eq. 5 allows an estimate for the diffusion coefficient for the Fe_2O_3 nanoparticles to be obtained and compared with the theoretically expected diffusion coefficient based on the Stokes–Einstein equation (eq. 3). From the experimental data (Fig. 6G), an experimental value for the diffusion coefficient, $D = 7.6 \times 10^{-11}$ m^2 s^{-1}, is calculated based on the assumption of a single electron being transferred per nanoparticle diffusing toward the electrode, $n = 1$. This estimate is consistent with the Stokes–Einstein value of approximately $D = 8.5 \times 10^{-11}$ m^2 s^{-1}. However, the Nernst layer assumption allows only estimates to be obtained when applied to sonovoltammetric limiting currents [33]. It is a striking observation that a value of $n = 1$ is required for the experimental results to be explained. The implication is that electron transfer between electrode and nanoparticle is slow in respect to the rate of mass transport. Further work will be required to reveal more mechanistic details of the electron transfer process between nanoparticles and electrode surface.

Finally, preliminary sonovoltammetric experiments have been conducted to explore the effect of solution pH on the interaction of the Fe_2O_3 nanoparticles with the ITO electrode surface. Figure 7 shows a comparison of sonovoltammograms obtained at pH 6, 8, and 9. The pH variation has a considerable impact on the adhesion and reactivity of Fe_2O_3 at the electrode surface. At pH 8, and even more pronounced at pH 9, peak-shaped sonovoltammetric reduction responses are detected for Fe_2O_3 adsorbed to the ITO electrode surface, even in the presence of ultrasound. Therefore, at low proton concentrations (pH > 7) and in the presence of phosphate and EDTA, the adhesion between Fe_2O_3 and ITO becomes strong enough to withstand cavitational cleaning. The magnitude of the peak-shaped reduction
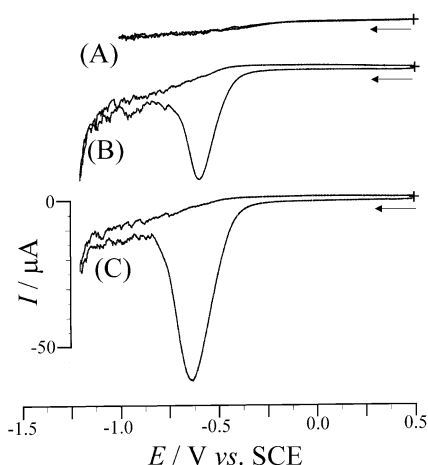

Fig. 7 Cyclic sonovoltammograms [24 kHz, 5 mm horn-to-electrode distance, 8 W cm^{-2}, scan rate 0.1 V s^{-1}, for (A) background substracted] obtained for the reduction of Fe_2O_3 nanoparticles at a 3×4 mm^2 ITO electrode immersed in aqueous 0.1 M phosphate buffer at (A) pH 6, (B) pH 8, and (C) pH 9 containing 10 mM EDTA and a concentration of 0.25 mM Fe in form of Fe_2O_3 nanoparticles.

response is increased compared to typical reduction peaks for Fe$_2$O$_3$ (compare Fig. 3) indicating the formation of a multi-layer deposit. Furthermore, the sonovoltammetric limiting current for the reduction of Fe$_2$O$_3$ nanoparticles is affected. At pH values >7 an increase by approximately a factor of 2 is observed, indicating a possible increase in the number of electrons transferred during the nanoparticle–electrode interaction.

CONCLUSIONS

It has been shown that nanoparticulate Fe$_2$O$_3$ can be detected directly in the aqueous solution phase in the presence of ultrasound. The presence of high rates of mass transport allows well-defined limiting currents to be detected consistent with diffusion of Fe$_2$O$_3$ nanoparticles toward the electrode and electron transfer reaction at the interface. Cavitational cleaning is preventing Fe$_2$O$_3$ nanoparticle deposition at ITO electrode surfaces at pH < 7. However, decreasing the concentration of protons causes a stronger adsorption and a more efficient electrochemical conversion.

ACKNOWLEDGEMENT

REFERENCES

1. S. Mann, J. Webb, R. J. P. Williams. *Biomineralisation*, VCH, Weinheim (1989).
2. W. Stumm. *Colloids Surf. A–Physicochem. Engineer. Aspects* **73**, 1 (1993).
3. W. Stumm, B. Sulzberger, J. Sinniger. *Croatica Chemica Acta* **63**, 277 (1990).
4. F. Wu and N.S. Deng. *Chemosphere* **41**, 1137 (2000).
5. V. V. Nikandrov, C. K. Grätzel, J. E. Moser, M. Grätzel. *J. Photochem. Photobiol. B–Biology* **41**, 83 (1997).
6. P. Mulvaney. In *Nanoparticles and Nanostrucured Films: Preparation, Characterisation and Applications*, J. H. Fendler (Ed.), p. 275, VCH, Weinheim, (1998).
7. A. N. Shipway, E. Katz, I. Willner. *ChemPhysChem* **1**, 18 (2000).
8. A. Henglein. *Ber. Bunsen Ges. Phys. Chem. Chem. Phys.* **99**, 903 (1995).
9. R. A. Mackay and J. Texter. *Electrochemistry in Colloids and Dispersions*, VCH, Weinheim (1992).
10. M. Heyrovsky, J. Jirkovsky, B. R. Muller. *Langmuir* **11**, 4293 (1995).
11. C. Boxall and W. J. Albery. *Phys. Chem. Chem. Phys.* **2**, 3641 (2000).
12. F. Scholz and B. Meyer. *Electroanal. Chem.* **20**, 1 (1998).
13. R. M. Cornell and U. Schwertmann. *The Iron Oxides—Structure, Properties, Reaction, Occurrences and Uses*, VCH, Weinheim (1996).
14. See, for example, Kh. Brainina, E. Neyman. *Electroanalytical Stripping Methods*, Wiley, New York (1993).
15. E. M. Andrade, F. V. Molina, G. J. Gordillo, D. Posadas. *J. Colloid Interf. Sci.* **165**, 459 (1994).
16. M. T. Mouhandess, F. Chassagneux, O. Vittori. *J. Electroanal.Chem.* **131**, 367 (1982).
17. M. T. Mouhandess, F. Chassagneux, O. Vittori, A. Accary, R. M. Reeves. *J. Electroanal. Chem.* **181**, 93 (1984).
18. T. Grygar. *J. Solid State Electrochem.* **2**, 127 (1998).
19. T. Grygar. *J. Solid State Electrochem.* **1**, 77 (1997).
20. T. Grygar, J. Subrt, J. Bohacek. *Coll. Czech. Chem. Commun.* **60**, 950 (1995).
21. P. Mulvaney, R. Cooper, F. Grieser, D. Meisel. *Langmuir* **4**, 1206 (1988).
22. C. H. Sorum. *J. Am. Chem. Soc.* **50**, 1263 (1928).

23. K. B. Holt, J. Del Campo, J. S. Foord, R. G. Compton, F. Marken. *J. Electroanal. Chem.* **513**, 94 (2001).
24. R. G. Compton, J. C. Eklund, F. Marken, T. O. Rebbitt, R. P. Akkermans, D. N. Waller. *Electrochim. Acta* **42**, 2919 (1997).
25. (a) G. A. Parks. *Chem. Rev*. **65**, 177 (1965); (b) M. A. Blesa, A. D. Weisz, P. J. Morando, J. A. Salfity, G. E. Magaz, A. E. Regazzoni. *Coord. Chem. Rev*. **196**, 31 (2000).
26. See, for example, *Gmelins Handbuch der Anorganishen Chemie*, 8th ed., Teil B, p. 773, Verlag Chemie, Berlin (1932).
27. M. Pourbaix. *Atlas of Electrochemical Equilibria*, p. 312, Cebelcor, Brussels (1974).
28. K. J. Laidler and J. H. Meiser. *Physical Chemistry*, p. 906, Houghton Mifflin, Boston (1999).
29. *CRC Handbook of Chemistry and Physics*, 74th ed., D. R. Lide (Ed.), CRC Press, London (1974).
30. R. G. Compton, J. C. Eklund, F. Marken. *Electroanalysis* **9**, 509 (1997).
31. See, for example, F. Marken, R. P. Akkermans, R. G. Compton. *J. Electroanal. Chem.* **415**, 55 (1996).
32. F. Marken, J. C. Eklund, R. G. Compton. *J. Electroanal. Chem.* **395**, 335 (1995).
33. H. A. O. Hill, Y. Nakagawa, F. Marken, R. G. Compton. *J. Phys. Chem*. **100**, 17395 (1996).